The authors thank the two reviewers for their thoughtful comments. A reply to each comment, including changes to the manuscript, is included below with the original comment in *italic* font and the reply in normal font.

Referee #1:

Section 3.3 – Can you address what, if any, losses of HCHO are expected on the inline particle filter (or even on the pressure controller)? Has this been tested? Were any laboratory calibrations conducted with the particle filters in place to make sure they match calibrations without filters?

Author reply:
The transmission of HCHO by the particle filter was tested with the calibration system and found to be 100%. We have seen no evidence of HCHO transmission issues with the pressure controller. The COFFEE pressure controller includes features that should improve its time response to changing [HCHO] relative to ISAF (Carzorla et al): the actuator has less exposed surface area, and the valve block is nickel-plated.

We added the following line to Section 3.3 to address this question:

> The transmission of HCHO by the particle filter was tested with the calibration system and found to be 100%.

P5L13 – Particle filters were used when "high aerosol loading is expected". Does this mean they were used in any non-laboratory deployment?

Author reply:
In practice, the filter has been used for all AJAX flights. The qualifying text was added to convey that flights with low aerosol loading (e.g. no boundary layer sampling) could operate without the filter and avoid the small loss of conductance from the filter. To clarify, the text has been changed to:

> The instrument is operated with an inline particle filter (Balston 9922-05-DQ) to minimize related measurement artifacts from high aerosol loading (see Sect. 4.5).

P5L15 – "The element retains 93% of the particles with a 0.01 um diameter." Does this mean it retains 93% of all particles larger than 0.01 um? Or is there some diameter over which it retains close to 100% of particles? What percentage of particle smaller than 0.01 um are retained, and do you expect this to make a difference in your analysis?

Author reply:
The statement is how the manufacturer describes their filter performance, with a retention

number for a specific particle diameter. Unfortunately they do not provide more detailed filter performance information. We recently had access to a CPC courtesy of the Jimenez Group from U. Colorado Boulder and sampled NASA DC-8 cabin air with and without the filter in place. The filter removed 99.98% of the particles.

Our objective for including the particle filter is to keep the prompt signal from Mie scattering sufficiently low that it doesn't dominate the signal time profile, and the current filter performs well in this regard. Versions of the filter with higher particle retention are available if we discover that is necessary, but currently we do not have evidence that higher retention is needed.

Section 3.3 – Is the inlet system here similar to the one shown in Fig. 5 of Carzorla et al? If not, describe the inlet used here. Is there anything in addition to the particle filter?

Author reply:
The inlet system is not the same as in Cazorla—it is a less sophisticated set-up. The Section 3.3 text that describes the inlet system:

> The current Alpha Jet inlet is a rear-facing stainless steel tube 9.5 mm OD (6 mm ID) that extends 17 cm beyond the bottom of the pod. 9.5 mm OD (6.35 mm ID) THV fluoropolymer tubing connects the inlet to the instrument chassis. The instrument is operated with an inline particle filter (Balston 9922-05-DQ) to minimize related measurement artifacts from high aerosol loading (see Sect. 4.5).

Section 3.5 –Clarify in the beginning of this section that both the exemplar fits and the gated spectra have their long-lived components removed before further analysis. The number system in this section makes it vague.

Author reply:
Currently the long-lived component is removed for the exemplar fits but not for the gated data processing, though this would be possible because of the 5 ns resolution binned data. Figures S2 and S3 are helpful in putting the size of the long-lived component into context—it is small and likely will always have a negligible effect on the gated data. The exemplar fitting routine, however, benefits from fitting a signal that decays to zero at the end of the time profile.

To better distinguish the exemplar fit data processing approach and the gated count approach, the following was added to the end of Sect. 3.5:

> In addition to the fitting-based data processing, HCHO mixing ratios can also be obtained from gated count data, as discussed in Sect. 3.5.3.

Section 3.5.1 – A figure in the supporting documents showing a raw spectrum and the long-lived component would be helpful in demonstrating how large this component is relative to the total signal. Or state it explicitly in the text.

Author reply:
Figures are a good idea for showing the contribution of the long-lived component. We added Figs. S2 and S3 that show time profiles and long-lived components for detection axis 2 and 1, respectively, for the same 1 s data period as in Fig. 5.

Section 3.5.2 – How sensitive is the shape of the HCHO exemplar to the concentration of HCHO used? Why use the profile with 25 ppbv HCHO, instead of an average of several concentrations (scaled, presumably)?

Author reply:
The shape of the HCHO fluorescence time profile is independent of the concentration of HCHO. The HCHO exemplar is derived from data with reasonably high (~25 ppbv) HCHO to ensure that HCHO dominates the shape of the time profile so that, when the air-only profile is subtracted, it is only a minor subtraction rather than a difference of two similarly large numbers. The high HCHO data is used to obtain the shape of the HCHO exemplar, but the corresponding calibration factor is obtained from the full calibration run, not just the high HCHO data.

To improve clarity, the following was added to the end of the "Obtaining the exemplars" subsection:

> Once the air and HCHO exemplars are obtained, they are used to fit laboratory calibration data with multiple HCHO concentrations using the two-step fit described below. The calibration factor unique to this HCHO exemplar is obtained from the linear regression of the HCHO added by the calibration system and the HCHO exemplar scaling factor, which is output of the fit.

P7L29 – What is the typical agreement between the two detection axes? State this.

Author reply:
The two axes generally agree well. We are still evaluating the utility of the two axes. To address the reviewer's point, we have added a figure (S4) to the supporting documents showing 60 s data from the two axes and a linear fit. The following text was also added:

> Data from the two axes generally agree well—Fig. S4 shows the cross plot of 60 s data from the two axes, along with a linear fit (slope = 0.98).

Section 3.5.3 – Consider making a figure for the supporting documents showing a

spectrum with shading to indicate where the gating occurs.

Author reply:
Figure S5 was added to show a time profile with the gated region shaded.

P10L11 – It's not clear where the 100 pptv value comes from: : :

Author reply:
We changed the text to improve clarity. It now reads:

> Currently no in-flight zeroing is performed for COFFEE. The 100 pptv term in the uncertainty is intended to account for any changes in the background signal over the ~2 hour duration AJAX flights. To date, we have not observed long time constant or high HCHO offset behavior with the COFFEE instrument that would be solved by in-flight zeroing.

Section 5 – Is there any reason to believe the "air exemplars" or the long-lived component might be different in-flight than on the ground? How consistent are the auxiliary measurements (i.e. detector internal pressure, laser head temperature) during vertical profiles?

Author reply:
By design, the "air exemplars" and the long-lived component are allowed to change in amplitude during flight in order to improve the fit. The engineering data in flight so far have given us no reason to suspect the instrument is behaving differently in flight than on the ground or in the lab. For example, both the power meter internal to the laser and our external power meter after the detection cell indicate the laser output is very stable through the flight, including through altitude changes.

Figures 4 and 5 – What concentrations of HCHO do these examples correspond to? Can you put this information either on the plot or in the caption?

Author reply:
The mixing ratios are 29 ppbv and 8 ppbv, respectively. This information has been added to the figure captions.

Table 1 – This table (and possibly Figure 11) could move to the supporting documents, as the focus of this paper is really on the instrument technique, and not on the measured spatial distribution of formaldehyde. You could give the details for the two flights in the caption for Figure 12 and leave out the rest.

Author reply:

Good suggestion-- Table 1 is now in the supporting document.

Technical comments:
P3L8 – "In practice, the laser is turned on: : :" is odd phrasing, as it implies that something else was supposed to happen in theory.

Author reply:
We agree. The phrasing is now improved:

> In flight operation, the laser turns on at the beginning of the flight and off at the end, with no other interaction.

P6L20 – "The fluorescence signal at the end of the bin-resolved data (_400 ns after the laser pulse): : :" Change to >400 ns, since you are taking the signal from 400-500 ns.

Author reply:
Done. The text is now:

> The fluorescence signal at the end of the bin-resolved data (>400 ns) is small but non-zero…

P6L24 – State what times bins 75-100 correspond to. Same comment for bins 87-100 on P6L27.

Author reply:
Done. Bins 75-100 correspond to 370-500 ns and bins 87-100 correspond to 430-500 ns. Note these times are relative to the start of the acquisition, and the laser pulse occurs at 50 ns.

Referee #2 (Alan Fried):

1. It's clear from paper that the new COFFEE instrument is more susceptible to scattered light from aerosols than ISAF, and this is dramatically illustrated in Fig. 9. Although ISAF is not the focus of the present study, as the measurements from COFFEE are an outgrowth of ISAF measurements and analysis, the authors may wish to comment on what the ISAF signals look like with particle filtering, if available. Also, it would be worth commenting if Drierite-filtered air was added to the inlet in flight, or is this not necessary from your lab testing?

Author reply:
COFFEE is indeed much more susceptible to scattered light from aerosols than ISAF due

to the much higher (~25x) laser power for COFFEE. For ISAF (Cazorla, et al., 2015), the 'full gate' data is affected by high aerosol loading (e.g. biomass burning plumes), but the prompt signal from scattering by particles is very effectively excluded by the 'delayed gate'. The following was added to Section 4.5 to clarify:

> The ISAF HCHO measurement is much less sensitive to the presence of particles due to its much lower (~25x) laser power, and utilizing a delayed gate for signal sampling is sufficient to exclude any artifact from scattering by particles.

Drierite-filtered air has not yet been used to provide an in-flight 'zero' for COFFEE, and the benefits/downsides of performing in-flight zeroing for these low flush-volume HCHO instruments is an active topic of discussion both within and outside our research group. Currently we believe, for these low flush-volume instruments, the downsides outweigh the benefits.

For COFFEE on the Alpha Jet, in comparison to ISAF operation on the NASA DC-8, there is a potentially greater benefit to in-flight zeroing due to the lower sample flows: COFFEE draws 2.3 sLm while ISAF, as currently configured on the DC-8 for the ATom campaign, subsamples ~4 sLm from a bypass flow of 14-30 sLm. That said, we have not observed long time constant or high HCHO offset behavior with the COFFEE instrument that would be solved by in-flight zeroing. Even with the lower 2.3 sLm sample flow, the COFFEE instrument flush time is rapid (170 ms, as discussed in Section 4.4). Ultimately, the 100 pptv term in the stated COFFEE measurement uncertainty is intended to conservatively account for any changes in the background signal over the ~2 hour duration AJAX flights.

We changed the text in Section 4.3 to read:

> Currently no in-flight zeroing is performed for COFFEE. The 100 pptv term in the uncertainty is intended to account for any changes in the background signal over the ~2 hour duration AJAX flights. To date, we have not observed long time constant or high HCHO offset behavior with the COFFEE instrument that would be solved by in-flight zeroing.

2. The authors on page 7 lines 28-29, indicate that "the final HCHO mixing ratio data product is produced by averaging the data from the two detection axes", it would be useful if the authors indicate what type of averaging was employed. Was a linear or weighted average employed? This could be important since as indicated on page 3 that detection axis 2 maximizes detection selectivity at the expense of deceased sensitivity, while axis 1 collects more fluorescence signal, potentially at the expense of selectivity. How are both attributes reflected in the final measurement?

Author reply:
This is a very good point, and one that is not yet fully resolved. Currently, for simplicity, we do an unweighted arithmetic mean of the two channels, but have considered other

options. One approach we have tried is averaging both channels to 1 minute data, taking the difference, and treating the difference as an 'error' term to be added to axis 1 before averaging the 1 s data from the two channels. Ultimately more field intercomparison data with ISAF or another HCHO instrument is necessary to decide which approach is superior. To improve clarity, the sentence now reads:

> The final HCHO mixing ratio data product is the arithmetic mean of the data from the two detection axes.

3. My final minor comment regards the terminology of Fig. 7 and its discussion in the manuscript involving the Allan deviation plot. Although David Allen first introduced this concept in 1966 for characterization of frequency standards, it was Peter Werle's seminal paper (P. Werle, R. Mücke, and F. Slemr, "The Limits of Signal Averaging in Atmospheric Trace-Gas Monitoring by Tunable Diode-Laser Absorption Spectroscopy (TDLAS)", Applied Physics B57, 131-139, 1993), that first brought this valuable tool to the attention of the atmospheric measurement community. Several of us are trying to acknowledge Peter's legacy in the literature by now referring such analysis and plots as "Allan-Werle" plots and analysis.

Author reply:
We are happy to recognize Peter Werle's contribution, and have changed the text to use "Allan-Werle" throughout.

A new non-resonant laser-induced fluorescence instrument for the airborne in situ measurement of formaldehyde

Jason M. St. Clair[1,2], Andrew K. Swanson[1,3], Steven A. Bailey[1], Glenn M. Wolfe[1,2], Josette E. Marrero[4], Laura T. Iraci[4], John G. Hagopian[5,6], Thomas F. Hanisco[1]

[1]Atmospheric Chemistry and Dynamics Laboratory, NASA Goddard Space Flight Center, Greenbelt, MD, 20771, USA
[2]Joint Center for Earth Systems Technology, University of Maryland Baltimore County, Baltimore, MD, 21228, USA
[3]Goddard Earth Sciences Technology and Research, Universities Space Research Association, Columbia, MD, 21046, USA
[4]Atmospheric Science Branch, NASA Ames Research Center, Moffett Field, CA, 94035, USA
[5]Lambda Consulting/Advanced Nanophotonics, Harwood, MD, 20776, USA
[6]Optics Branch, Instrument Systems and Technology Division, NASA Goddard Space Flight Center, Greenbelt, MD, 20771, USA

Correspondence to: Jason M. St. Clair (jason.m.stclair@nasa.gov)

Abstract. A new in situ instrument for gas-phase formaldehyde (HCHO), COmpact Formaldehyde FluorescencE Experiment (COFFEE), is presented. COFFEE utilizes non-resonant laser-induced fluorescence (NR-LIF) to measure HCHO, with 300 mW of 40 kHz 355 nm laser output exciting multiple HCHO absorption features. The resulting HCHO fluorescence is collected at 5 ns resolution, and the fluorescence time profile is fit to yield the ambient HCHO mixing ratio. Typical 1-σ precision at ~0 pptv HCHO is 150 pptv for 1 s data. The compact instrument was designed to operate with minimal in-flight operator interaction and infrequent maintenance (1-2 times per year). COFFEE fits in the wing pod of the Alpha Jet stationed at NASA Ames Research Center and has successfully collected HCHO data on 27 flights through 2017 March. The frequent flights, combined with a potentially long-term data set, makes the Alpha Jet a promising platform for validation of satellite-based column HCHO.

1 Introduction

Formaldehyde (HCHO) is an abundant, photochemically influential trace species in the Earth's atmosphere. Primary sources of HCHO include biomass burning (Akagi et al., 2011; Andreae and Merlet, 2001) and fossil fuel combustion (Anderson et al., 1996; Luecken et al., 2012; Olaguer et al., 2009), but these are dwarfed by secondary production from the photochemical oxidation of volatile organic compounds (VOC). This secondary source is dominated by the locally abundant VOC(s): CH_4 in the remote atmosphere, isoprene in biogenically active regions (Palmer et al., 2003; Shim et al., 2005), and unsaturated (Parrish et al., 2012) VOCs in regions with large anthropogenic VOC emissions. HCHO loss occurs via photolysis and reaction with OH, resulting in a daytime atmospheric lifetime of a few hours. Mixing ratios of HCHO vary

from tens of parts per trillion (pptv) in the remote atmosphere (Fried et al., 2003) to a few parts per million by volume (ppmv) in biomass burning plumes (Akagi et al., 2014), with typical values in the 50 pptv to 10 ppb range. Elevated HCHO, due to its limited atmospheric lifetime, is indicative of recent VOC oxidation, and in the upper troposphere and lower stratosphere (UT/LS) it suggests recent convective transport (Apel et al., 2012; Fried et al., 2008b, 2016). Measurements of HCHO are valuable both as a tracer of recent VOC oxidation, and also due to its role in HO_x/O_3 chemistry (Jaeglé et al., 2001).

Atmospheric HCHO is measured using a variety of airborne instrumental methods, including mass spectrometry (Warneke et al., 2011), wet chemistry (Aiello and Mclaren, 2009; Junkermann and Burger, 2006; Lazrus et al., 1988), absorption spectroscopy (Baidar et al., 2013; Catoire et al., 2012; Richter et al., 2015; Washenfelder et al., 2016; Weibring et al., 2006; Yokelson et al., 1999), and laser-induced fluorescence (LIF) (Cazorla et al., 2015; Hottle et al., 2009; Mohlmann, 1985). In addition to airborne observations, total column HCHO is measured by satellite (Chance et al., 2000; Steck et al., 2008), making HCHO one of the few VOCs observable from space. Numerous measurement technique reviews and instrument intercomparisons are available (Fried et al., 2008a; Hak et al., 2005; Kaiser et al., 2014; Zhu et al., 2016).

Traditionally, LIF measurements of HCHO have used a wavelength-tunable excitation laser to dither on and off the HCHO absorption feature, using the difference in signal to calculate the HCHO mixing ratio. The benefit of this approach is that the differential signal excludes any broadband background fluorescence from interfering with the HCHO measurement. The downside is that it requires either a large laser system unsuited for compact airborne instrumentation (Mohlmann, 1985), or a custom, high cost fiber laser (Cazorla et al., 2015; Hottle et al., 2009). We present a new approach to measurement of HCHO by non-resonant laser-induced fluorescence (NR-LIF), using a fixed wavelength UV industrial laser at 355 nm to excite multiple HCHO absorption features simultaneously. Lacking the tunability and narrow linewidth necessary to dither on and off a single absorption feature, selectivity to HCHO is instead obtained using specialized fluorescence optical filters, and by employing high temporal resolution data acquisition to uniquely identify HCHO by its characteristic fluorescence lifetime.

The new NR-LIF HCHO instrument, COmpact Formaldehyde FluorescencE Experiment (COFFEE), was designed specifically to join the payload of the Alpha Jet Atmospheric eXperiment (AJAX) out of NASA Ames Research Center in Mountain View, CA. The robust optomechanical design of the COFFEE instrument, combined with its simple and reliable operation, makes the instrument ideal for long-term deployment to NASA Ames with minimal maintenance. The routine, long-term nature of the AJAX project, with flights approximately every two weeks, makes the Alpha Jet a good platform for monitoring seasonal and long-terms trends, as well as providing an extensive in situ data set for satellite validation.

2 Measurement technique

The COFFEE instrument uses NR-LIF for the detection of HCHO. Previous LIF-based instruments for atmospheric HCHO, such as the NASA In Situ Airborne Formaldehyde (ISAF) instrument (Cazorla et al., 2015), have used a narrow bandwidth, state-specific tunable excitation laser to target a specific absorption feature. COFFEE, in contrast, employs a moderate bandwidth (full width at half maximum (FWHM) ~ 1 nm) fixed wavelength laser that excites multiple HCHO absorption features. The HCHO absorption cross section from Co et al. (2005), averaged to 0.001 nm resolution, is shown with the overlapping COFFEE laser output in the top panel of Fig. 1. The commercial off-the-shelf fixed wavelength laser is both less expensive and operationally more reliable than the narrow bandwidth tunable laser. In flight operation, the laser turns on at the beginning of the flight and off at the end, with no other interaction.

HCHO fluorescence occurs over the ~355-550 nm wavelength range, as shown in Fig. 1, bottom panel. COFFEE has two detectors for collecting the banded fluorescence. Optical filter details are included in Sect. 3.2. Detection axis 1 uses a band pass filter centered at 450 nm (Fig. S1) to collect as much HCHO fluorescence as possible while excluding the primary sources of background counts (chamber, Raman, and Rayleigh scatter). Detection axis 2 (Fig. 1, bottom panel) utilizes a multi-band pass filter that selectively transmits at HCHO fluorescence wavelengths, maximizing detection selectivity at the expense of decreased sensitivity.

Other LIF-based instruments for atmospheric HCHO (Cazorla et al., 2015; Hottle et al., 2009) collect fluorescence using a long pass filter to exclude scatter, and achieve measurement selectivity by alternately tuning the narrow bandwidth laser on and off a HCHO absorption feature. The fixed wavelength laser in COFFEE cannot provide on and off line measurements. Measurement specificity to HCHO is instead achieved by acquiring the time-resolved fluorescence signal, 5 ns bins for 500 ns, and leveraging the unique fluorescence lifetime of HCHO in data processing. The details of data acquisition and data processing are discussed in Sect. 3.4 and 3.5, respectively.

3 Instrument description

3.1 Laser

A Spectra-Physics Explorer (EXPL-355-300-E, Fig. 2, item A) provides 300 mW of 355 nm of pulsed radiation at 40 kHz (adjustable 20-60 kHz). The laser is actively Q-switched, with a Nd:YVO_4 gain medium pumped by a single 808 nm diode to provide the 1064 nm fundamental wavelength. UV output at 355 nm is created using two intracavity lithium triborate crystals for second and third harmonic generation. The pulse width (FWHM) is <15 ns, and the bandwidth is ~ 1 nm. The

St Clair, Jason M. (…, 9/22/2017 2:16 PM
Deleted: In practice, the laser is turned on at the beginning of the flight and off at the end, with no other interaction.

laser is compact, with head dimensions 16.5 cm x 9.5 cm x 5.4 cm (0.9 kg) and power supply dimensions 16.4 cm x 13 cm x 6.6 cm (1.2 kg). Computer control is via RS232.

The laser head requires proper thermal management for the laser to perform to specification. 40 W of heat must be removed from the laser head at its maximum operating temperature of 308 K. Two thermal electric cooler (TEC) devices (TE Technology) provide thermal control of the laser head. The laser side of the TECs is controlled to 303 K, and the other side of the TECs are in thermal contact with the optical plate and heat sinks mounted to the underside of the optical plate.

3.2 Optical system

The optical layout of the instrument (Fig. 2, item B) is shown in more detail in Fig. 3. The entire optical system is contained on the optical plate in a single plane. The plate was machined out of 13 mm thick 6061 aluminum and is secured to the chassis at four points utilizing Sorbothane vibration isolation bushings. The plate is heated to 303 K.

The laser beam is directed by two antireflection (AR)-coated dielectric mirrors (CVI Laser Optics) into the detection cell. A collimating lens (F= 100 mm, Thorlabs) and a λ/2 wave plate (AR-coated, OptiSource), the latter used to minimize the Raman scattering directed at the photomultiplier tubes (PMTs), are positioned in between the turning mirrors. The detection cell is very similar to the cell in ISAF (Cazorla et al., 2015), with the main differences being the number and orientation of the PMTs, and the optical filters used. The beam enters and exits the cell through AR-coated fused silica windows (CVI Laser Optics) that are mounted at a 3.5° angle to prevent surface reflections from reaching the PMTs. Inside the cell, the beam continues through a series of circular baffles, 4 before the detection volume and 3 after, which drastically reduce stray light. The baffle apertures are progressively larger along the beam propagation path (2.5 mm, 3.0 mm, 3.5 mm). The baffles adjacent to the detection volume are coated with a carbon nanotube coating (Hagopian, 2011); the other baffles are laser-cut and painted black (Lenox Laser). The interior of the detection cell is coated with a molybdenum oxide treatment (Insta-Black 380, EPI), to further eliminate stray light.

On two sides of the detection cell, aspheric lenses (NA=0.66, AR-coated, Edmund Optics) image the volume where the laser beam and main gas flow cross. From each lens, the image is reflected 90° by a turning mirror (right angle prism dielectric, Thorlabs) and passed through a series of optical filters before being partially focused by a lens (F = 75 mm, AR-coated, Thorlabs) onto a photomultiplier tube (PMT) (Hamamatsu H7360-02 MOD). The optical filters differ between the two PMTs. Arranged in order from the aspheric lens to the PMT, axis 1 contains an AR-coated 370 nm long pass absorption filter (Hoya Candeo Optronics), a 450 nm, 70 nm wide band pass interference filter (Semrock), and a 395 nm long pass absorption filter (Edmund Optics). Axis 2 uses a 400 nm long pass interference filter (Omega Optical), an AR-coated 370

nm long pass absorption filter (Hoya Candeo Optronics), a custom 11-band band pass interference filter (Semrock), and a 395 nm long pass absorption filter (Edmund Optics). The 11-band filter was designed to selectively transmit formaldehyde fluorescence while reducing the background. After the detection cell, a beam sampler (Thorlabs) splits the beam, and the main beam continues to a beam dump. The beam sampler reflection is directed to a power meter consisting of a diffuser (Thor DGUV10-600), absorption filter (Thorlabs FGUV11), and an amplified photodiode (OSI 555-UV).

3.3 Gas handling

The fundamental design consideration for the instrument sample flow is to minimize the potential for the adsorption/release of HCHO to/from exposed surfaces (Cazorla et al., 2015; Wert et al., 2002). To that end, all surfaces that deliver gas to the detection cell are either fluorocarbon (FEP, THV) or fluorocarbon-coated (FluoroPel, Cytonix). The current Alpha Jet inlet is a rear-facing stainless steel tube 9.5 mm OD (6 mm ID) that extends 17 cm beyond the bottom of the pod. 9.5 mm OD (6.35 mm ID) THV fluoropolymer tubing connects the inlet to the instrument chassis. The instrument is operated with an inline particle filter (Balston 9922-05-DQ) to minimize related measurement artifacts from high aerosol loading (see Sect. 4.5). The filter housing is Kynar (polyvinylidene fluoride) and the filter element is a microfiber with a fluorocarbon resin binder. The element retains 93% of the particles with a 0.01 µm diameter. The transmission of HCHO by the particle filter was tested with the calibration system and found to be 100%.

St Clair, Jason M. …, 9/22/2017 10:44 AM
Deleted: The instrument is operated with an inline particle filter (Balston 9922-05-DQ) when high aerosol loading is expected in order to minimize related measurement artifacts (see Sect. 4.5).

St Clair, Jason M. (…, 9/22/2017 2:07 PM
Deleted: . ... [1]

Inside the instrument, 5 cm of 9.5 mm OD PFA tubing connects from the chassis to a pressure controller, and 15 cm of 9.5 mm OD PFA tubing connects from the pressure controller to the detection cell. The pressure controller (Fig. 2, item C) is an actuator (iQ Valve) coupled with a custom valve block, and is heated to 308 K. The detection cell pressure is regulated to 10.7 kPa. The main flow passes directly down through the detection cell and out of the chassis to the vacuum pump (Vacuubrand MD-1, Fig. 2 item D). A small amount of air is pulled through the laser baffle arms to flush that volume, and the flow is combined with the main flow (after the detection cell) before exiting the chassis. In lab, the instrument sampling flow is 2.3 sLm.

3.4 Data acquisition

Data acquisition and instrument control is conducted by a National Instruments CompactRIO system, hereafter RIO (Fig. 2, item E). The RIO consists of a main processor module (running a realtime operating system) and a backplane driven by a field programmable gate array (FPGA). Additional plugin modules add I/O. NI 9205 and NI 9264 modules provide analog input and output, respectively. Two channels of a NI 9402 high speed digital I/O module are programmed as 5 ns resolution counters, with each PMT having its own counter. The counters are triggered by the OptoSync from the laser (30-100 ns after the laser pulse), which provides a TTL pulse closer in coincidence with the laser pulse than obtained from the laser trigger

out. In order for the PMT signals to arrive after the counters are triggered, they are delayed by 50 ns with a passive delay circuit (Data Delay Devices, 1515 series).

Data for each PMT channel are acquired in two ways: 1) integrated every 0.1 s with non-gated (continuous) and gated data streams, which are used primarily for diagnostic purposes, and 2) integrated every 1 s and time-resolved to 100 discrete time bins, each 5 ns wide, that cover the 500 ns immediately following the counter trigger. The 5 ns time-resolved data are the key to the data processing approach necessary to minimize measurement artifacts with the NR-LIF approach, as will be discussed in Sect. 3.5, and is used to produce the HCHO mixing ratio data product. Diagnostic data (laser power, pressures, temperatures, etc.) are also recorded every 1 s.

3.5 Data processing

HCHO mixing ratios are obtained using the 5 ns bin time-resolved profiles from the two detection axes. The data processing consists of three steps, each done independently for the two detection axes: 1) subtraction of the minor 'long-lived' component from the time profile; 2) two-parameter nonlinear least squares fit of the data using profiles (hereafter referred to as exemplars) that represent the HCHO and non-HCHO (chamber scatter, Raman and Rayleigh scatter, fluorescence of optics, etc.) contributions to the observed profile; 3) one-parameter nonlinear least squares fit with the non-HCHO contribution fixed from the previous two-parameter fit, and only the HCHO contribution allowed to vary. The second pass fit with only one parameter improves the precision of the measurement. In addition to the fitting-based data processing, HCHO mixing ratios can also be obtained from gated count data, as discussed in Sect. 3.5.3.

3.5.1 Long-lived component

The fluorescence signal at the end of the bin-resolved data (>400 ns) is small but non-zero, and changes in this 'long-lived' signal do not scale with changes in the non-HCHO 'air' exemplar, necessitating a separate treatment. The long-lived signal has a longer fluorescence lifetime than HCHO, which permits fitting and removal of the long-lived signal without interference from ambient HCHO. For detection axis 1, an empirical profile determined from a laboratory run is scaled to fit the observed 1 Hz data using a single parameter least squares fit to the observed profile from bin 75 to bin 100 (370-500 ns), and the scaled profile is subtracted from the observed data before performing the exemplar fits. For detection axis 2, the long-lived signal is smaller than for axis 1 by a factor of ~ 6 and is stable over the last ~15 bins, and so a simpler treatment is used: the observed 1 Hz profile is averaged from bin 87 to bin 100 (430-500 ns) and the mean is subtracted as a constant from all bins in the observed profile before performing the exemplar fits. Examples of time profile data for both detection axes along with their respective long-lived components are shown in Fig. S2 and Fig. S3. All fitting and exemplar creation is done using data with the long-lived component removed.

St Clair, Jason M. …, 9/22/2017 10:46 AM
Deleted: ~

St Clair, Jason M. …, 9/22/2017 10:46 AM
Deleted: after the laser pulse

3.5.2 Exemplar fits

Obtaining the exemplars

The representative time profiles, or exemplars, are determined from laboratory calibration runs where the instrument samples clean, dry air (typically UHP dry air) with varied amounts of HCHO added. The 'air exemplar', which represents all non-HCHO contributions to the observed profile, is obtained by time-averaging the observed profile when no HCHO is added to the dry air. Figure 4 shows the profiles involved in creating the 'HCHO exemplar'. The HCHO exemplar (Fig. 4, red dashed) is obtained by time averaging the observed profile (Fig. 4, cyan circles) during the calibration period of maximum HCHO (typically 25-30 ppbv) and subtracting the air exemplar (Fig. 4, blue dashed) from the time-averaged profile. The highest HCHO period is used so that HCHO dominates the shape of the observed profile. Once the air and HCHO exemplars are obtained, they are used to fit laboratory calibration data with multiple HCHO concentrations using the two-step fit described below. The calibration factor unique to this HCHO exemplar is obtained from the linear regression of the HCHO added by the calibration system and the HCHO exemplar scaling factor, which is output of the fit.

Two-parameter exemplar fit

An example two-parameter exemplar fit is shown in Fig. 5. The observed profile (Fig. 5, cyan circles), with the long-lived component removed, is fit with a linear combination of the air exemplar and the HCHO exemplar. The fit parameters are the scalar multipliers applied to the exemplars: the scaled air exemplar (Fig. 5, blue dashed) and scaled HCHO exemplar (Fig. 5, red dashed). The least squares optimization is performed on the data from bin 13 to bin 60, with the fit window chosen to maximize data precision and fit quality, as determined by visual inspection of fit residuals. The optimized fit for the bin 13-60 window is shown in black.

One-parameter exemplar fit

The first step of the one-parameter fit applies a 21 s median filter to the vector of air exemplar fit scalars from the two-parameter fit. The smoothed vector is then used in a one-parameter fit where the air exemplar contribution is fixed to the air exemplar scaled by the smoothed vector, and the HCHO exemplar scaling factor is allowed to vary. The result is a higher precision fit, and is possible because the phenomena that comprise the 'air exemplar' contribution to the observed profile (chamber scatter, Raman and Rayleigh scatter, fluorescence of optics, etc.) do not change rapidly. The output of the one-parameter fit, the HCHO exemplar scalar, is directly proportional to HCHO mixing ratio. HCHO data in pptv are obtained by applying a calibration factor, unique to the HCHO exemplar used, to the fit output. The final HCHO mixing ratio data product is the arithmetic mean of the data from the two detection axes. Data from the two axes generally agree well—Fig. S4 shows the cross plot of 60 s data from the two axes, along with a linear fit (slope = 0.98).

St Clair, Jason M. …, 9/22/2017 10:48 AM
Deleted: produced by averaging the data from the two detection axes

3.5.3 Data processing with gated count data

In addition to data processing with exemplar profiles, time-gated 1 Hz data derived from the time-resolved profiles can be used to obtain HCHO, with higher measurement precision than is achieved with the exemplar fits. For example, a calibration experiment yields, for 1 s data and 0 pptv added HCHO, standard deviations of 150 pptv for the one-parameter exemplar fit (175 pptv for the two-parameter fit only) and 130 pptv for the gated count data (167 pptv for ungated count data). The time-gated data excludes much of the prompt signal from scatter by summing counts from bin 24 to bin 100 (115 ns to 500 ns). Using the same laboratory calibration experiment as an example: with no HCHO added, the gate excluded 89% (450 nm filter detection axis) and 95% (multi-band pass axis) of the total signal in the first 500 ns from the trigger. More of the HCHO signal is retained due to its fluorescence lifetime: 73% of the HCHO signal is excluded by the gate. Figure S5 shows the time profile from Fig. 5 with the gate window shaded. Gated count 10 Hz data, as well as ungated count 10 Hz data, can be used to obtain HCHO mixing ratios. The 10 Hz data are used only for diagnostic purposes, e.g. the instrument flush time experiment in Sect. 4.4.

The count signal is converted to HCHO mixing ratio using a linear relationship determined from laboratory calibrations, with the slope being the instrument sensitivity to HCHO (discussed in Sect. 4.1) and the intercept being the signal at HCHO = 0 pptv, comprised of the same signal sources as the air exemplar: chamber scatter, Raman and Rayleigh scatter, and fluorescence of optics. While the count-derived HCHO data are higher precision than the exemplar fit-derived HCHO data, the count-derived data are potentially more prone to measurement error from changes in background signal due to changes in alignment, degradation of optics, the presence of aerosol (Mie scattering), or from unknown fluorescing compounds. In contrast, ISAF (Cazorla et al., 2015) is immune to these changes in background due it its measurement of online and offline signal. Currently the count-derived HCHO data are only used for diagnostic purposes.

4 Performance

4.1 Sensitivity

The sensitivity of each detection axis to a given amount of HCHO is a function of a number of instrument parameters: laser power, collection optics efficiency, fluorescence optical filter transmission, and PMT response. As for ISAF, none of the instrument parameters that affect instrument sensitivity are expected to degrade on a time scale shorter than years. The HCHO calibration of the instrument has been measured 2-3 times per year, and will be measured at least once a year in the future to track any changes in sensitivity.

Calibration is performed using measured flows from two cylinders, one containing ultra-high purity (UHP) air further purified with a Drierite/molecular sieve scrubber and the other a ~500 ppbv mixture of HCHO in N_2. The exact concentration of the HCHO mixture in all of our HCHO standard cylinders is measured yearly using IR absorption, with less frequent verification of the IR measurement by long-path UV absorption. Details of the HCHO cylinder assessment via IR and UV absorption are available in Cazorla et al. (2015). HCHO calibration accuracy for COFFEE is determined by the uncertainty in the HCHO standard concentration as well as the uncertainty in the gas flow dilution described below, and is estimated to be ±10%.

For calibration, flow of the HCHO standard is sequentially set to 3-5 different flows in the range 0-50 standard cm^3 min^{-1} (sccm) and is added to a carrier flow of UHP air, typically 3-5 standard L min^{-1} (sLm). The instrument draws ~ 2.3 sLm and the remaining gas flow exhausts to the room before the pressure controller—the additional flow improves the time response of the calibration system. Typical calibration data for detection axis 2 is shown in Fig. S6.

St Clair, Jason M. …, 9/22/2017 10:49 AM
Deleted: S2

Instrument sensitivity to HCHO differs for the two detection axes primarily due to their respective optical filter transmission, with axis 1 more sensitive than axis 2. The gated count sensitivities for axis 1 and axis 2 are 0.29 counts s^{-1} mW^{-1} $ppbv^{-1}$ and 0.13 counts s^{-1} mW^{-1} $ppbv^{-1}$, respectively. The ungated sensitivities for axis 1 and axis 2 are 0.98 counts s^{-1} mW^{-1} $ppbv^{-1}$ and 0.47 counts s^{-1} mW^{-1} $ppbv^{-1}$, respectively. For comparison, the ISAF sensitivity is 75 counts s^{-1} mW^{-1} $ppbv^{-1}$ for its typical 100 mbar operating pressure. Power normalized sensitivities are significantly lower (>100x) for COFFEE than the ISAF instruments primarily due to the less efficient overlap of the COFFEE laser output with the HCHO absorption lines.

4.2 Precision

Measurement precision is the dominant component of overall measurement uncertainty at low (< 700 pptv) mixing ratios. The standard deviation using data from two laboratory calibration experiments is shown in Fig. 6. At [HCHO] = 0 ppbv, the precision is ±130 pptv in 1 s and ±60 pptv in 10 s. Relative measurement precision improves with increasing HCHO, as shown in Fig. S7 using the same calibration data. The largest source of noise for COFFEE HCHO is Raman and Raleigh scattering of the excitation beam by air. Chamber scatter accounts for ~15% of signal (2 counts s^{-1} mW^{-1}) for axis 1 and ~25% of signal (1 count s^{-1} mW^{-1}) for axis 2 at 10.7 kPa and HCHO = 0 ppbv, with the remaining signal from Raman and Raleigh scatter.

St Clair, Jason M. …, 9/22/2017 10:49 AM
Deleted: S3

Precision should improve as data are time-averaged. In practice, the benefit of additional time-averaging ceases when the data variability is no longer dominated by random noise. The Allan-Werle deviation plot shown in Fig. 7 demonstrates this point for COFFEE HCHO data from a laboratory calibration with ~5 ppbv HCHO, processed with the two-parameter exemplar fit. The precision of the HCHO data improves with averaging until reaching a 250 s averaging time basis,

implying that the signal-to-noise ratio for COFFEE measurements will improve from 1 s data to 10 s data, and again to 1-minute data. Fitting the decreasing linear (in log-log space) portion of the data yields a slope of -0.5, which is consistent with the data variability being dominated by white noise on time scales shorter than 250 s. The full fit-based data processing includes an additional step beyond the two-parameter fit, and a similar Allan-Werle deviation analysis gives a slope of -0.4. The difference is likely due to the median filtering applied to the air exemplar scalar before conducting the one-parameter fit.

4.3 Measurement uncertainty

The overall measurement uncertainty for COFFEE HCHO is estimated to be ± (20% of [HCHO] + 100 pptv). As discussed in Sect. 4.1, the calibration uncertainty is ±10% of [HCHO]. The additional 10% uncertainty is added to conservatively account for unquantified sources of error such as unknown signal sources other than HCHO and any fit biases. Additional and more extensive opportunities for instrument intercomparison in situ will likely reduce the need for this extra uncertainty. Currently no in-flight zeroing is performed for COFFEE. The 100 pptv term in the uncertainty is intended to account for any changes in the background signal over the ~2 hour duration AJAX flights. To date, we have not observed long time constant or high HCHO offset behavior with the COFFEE instrument that would be solved by in-flight zeroing.

St Clair, Jason M. (…, 9/22/2017 1:35 PM
Deleted: The 100 pptv term is to account for changes in the background signal that are not fully accounted for by the scaled air exemplar when performing the two-parameter fit.

4.4 Time response

Instrument time response directly affects the ability to resolve fine structure in atmospheric HCHO, and can affect measurement accuracy in regions of high HCHO contrast such as biomass burning plumes. Understanding the instrument time response is critical to properly interpreting the in situ data. Assuming a volume of 60 cm^3 and a volumetric flow of 29 L min^{-1} (2.3 sLm, 303 K, 10.7 kPa), the e-fold flush time of COFFEE was estimated to be 125 ms. The actual time response of the instrument was measured by introducing narrow time pulses of HCHO into the instrument and fitting the signal decay, as shown in Fig. 8. A low volume, rapidly switching valve (The Lee Company, IEP series) provided a 10 ms pulse of HCHO every 2 minutes into a flow of UHP air. The HCHO signal after the pulse was fit with an exponential decay, yielding an empirical e-fold flush time of 170 ms, 45 ms slower than the flush time estimated from volume and flow rate alone. Typically the data rate reported by COFFEE is 1 Hz, and therefore the 170 ms 1/e instrument response time will have a very limited effect on the observed HCHO data.

4.5 Measurement interference from aerosol

Mie scattering from the presence of aerosol increases the prompt signal (< 75 ns after trigger) detected by COFFEE. The additional prompt signal complicates the exemplar fitting routine by altering the profile shape of the non-HCHO component in the data time profile. To avoid the presence of Mie scattering, all ambient sampling with COFFEE is conducted through an in-line particle filter. An example of the error experienced by COFFEE from unfiltered ambient sampling is shown in Fig. 9. COFFEE and ISAF were installed in an office trailer on the roof of a NASA Goddard laboratory building, and both instruments sampled ambient air through the same ¼" OD PFA tubing mounted on the roof of the trailer. With COFFEE sampling through the particle filter, the instruments agree well sampling ambient air, room air, and Drierite-filtered air. The measurements do not agree as well, with a difference of >1 ppbv, for periods of ambient sampling without a particle filter on COFFEE, shaded gray. The ISAF HCHO measurement is much less sensitive to the presence of particles due to its much lower (~25x) laser power, and utilizing a delayed gate for signal sampling is sufficient to exclude any artifact from scattering by particles.

5 Field deployment

5.1 Alpha Jet integration

COFFEE was designed specifically for integration onto the Alpha Jet (H211, LLC) stationed at NASA Ames—Moffett Field to participate in the Alpha Jet Atmospheric eXperiment (AJAX) (Hamill et al., 2016). The Alpha Jet carries four wing pods, with the outboard pods containing fuel and the inboard pods available for instrumentation. Each instrument wing pod has a usable volume of ~0.1 m^3 and a maximum payload weight of 136 kg. COFFEE mounts in the mid-body of the left wing pod, as shown in Fig. 10. The instrument chassis (Fig. 2, item F) and pump (Fig. 2, item D) attach to a rack designed for use in the wing pods (Fig. 2, item G) and the rack then slides into the pod mid-body, making removal of the instrument straightforward for infrequent maintenance.

5.2 Flight data

The first flight of COFFEE on the Alpha Jet was on 2015 December 15. Since then, COFFEE has operated on 27 AJAX flights through March 2017, with data coverage predominately in the Bay Area and Central Valley of California. Figure 11 shows a map with overlaid flight tracks for all the AJAX flights with COFFEE, and Table S1 lists the dates and objectives for each of the 27 flights. During this period COFFEE returned to GSFC just three times for maintenance, typically timed to coincide with aircraft maintenance.

St Clair, Jason M. (…, 9/22/2017 1:36 PM
Deleted: 1

Data from AJAX Flight 185 on 2016 April 19 are shown in Fig. 12 as an example of COFFEE HCHO performance. The flight included two spiral profiles, one over the San Joaquin Valley near Merced, CA (37.38° N, 120.6° W) and one directly west, offshore over the Pacific Ocean (37.17° N, 123.2° W). The altitude profiles of HCHO for the two spirals are shown in the bottom panel of Fig. 12 for 10 s data. The onshore and offshore profiles are similar between 4 km and 9 km, and diverge considerably below 2 km as local photochemistry drives HCHO production over land. The profiles serve as a demonstration of the data set available for validation of HCHO satellite retrievals using routine AJAX flights over targeted profile locations.

6 Summary

The NR-LIF technique utilized in COFFEE has proven to be a viable, operationally robust approach to measuring gas phase in situ HCHO. While not achieving the sensitivity of a state-selective LIF instrument such as ISAF (Cazorla et al., 2015), the NR-LIF technique provides adequate precision (1-σ of 150 pptv for 1 s data at 0 pptv HCHO) for most scientific pursuits, with a lower cost, highly reliable laser. COFFEE data from over two dozen AJAX flights spread over 15 months have demonstrated the potential utility of the aircraft platform for validation of satellite-based total column HCHO.

7 Data availability

AJAX data are available upon request. Data contact: Laura Iraci (Laura.T.Iraci@nasa.gov).

The Supplement related to this article is available online.

Acknowledgements. Funding was provided by the Goddard Internal Research and Development (IRAD) program and NASA (NNH16ZDA001N-UACO). J. E. Marrero gratefully acknowledges funding from the NASA Postdoctoral Program.

References

Aiello, M. and McLaren, R.: Measurement of airborne carbonyls using an automated sampling and analysis system, Environ. Sci. Technol., 43, 8901–8907, doi:10.1021/es901892f, 2009.

Akagi, S. K., Yokelson, R. J., Wiedinmyer, C., Alvarado, M. J., Reid, J. S., Karl, T., Crounse, J. D. and Wennberg, P. O.: Emission factors for open and domestic biomass burning for use in atmospheric models, Atmos. Chem. Phys., 11, 4039–4072, doi:10.5194/acp-11-4039-2011, 2011.

Akagi, S. K., Burling, I. R., Mendoza, A., Johnson, T. J., Cameron, M., Griffith, D. W. T., Paton-Walsh, C., Weise, D. R., Reardon, J. and Yokelson, R. J.: Field measurements of trace gases emitted by prescribed fires in southeastern US pine forests using an open-path FTIR system, Atmos. Chem. Phys., 14, 199–215, doi:10.5194/acp-14-199-2014, 2014.

Anderson, L. G., Lanning, J. A., Barrell, R., Miyagishima, J., Jones, R. H. and Wolfe, P.: Sources and sinks of formaldehyde and acetaldehyde: An analysis of Denver's ambient concentration data, Atmos. Environ., 30, 2113–2123, doi:10.1016/1352-2310(95)00175-1, 1996.

Andreae, M. O. and Merlet, P.: Emission of trace gases and aerosols from biomass burning, Global Biogeochemical Cycles, 15, 955–966, doi:10.1029/2000GB001382, 2001.

Apel, E. C., Olson, J. R., Crawford, J. H., Hornbrook, R. S., Hills, A. J., Cantrell, C. A., Emmons, L. K., Knapp, D. J., Hall, S., Mauldin, R. L., Weinheimer, A. J., Fried, A., Blake, D. R., Crounse, J. D., St. Clair, J. M., Wennberg, P. O., Diskin, G. S., Fuelberg, H. E., Wisthaler, A., Mikoviny, T., Brune, W. and Riemer, D. D.: Impact of the deep convection of isoprene and other reactive trace species on radicals and ozone in the upper troposphere, Atmos. Chem. Phys., 12, 1135–1150, doi:10.5194/acp-12-1135-2012, 2012.

Baidar, S., Oetjen, H., Coburn, S., Dix, B., Ortega, I., Sinreich, R. and Volkamer, R.: The CU Airborne MAX-DOAS instrument: Vertical profiling of aerosol extinction and trace gases, Atmos. Meas. Tech., 6, 719–739, doi:10.5194/amt-6-719-2013, 2013.

Catoire, V., Bernard, F., Mébarki, Y., Mellouki, A., Eyglunent, G., Daële, V. and Robert, C.: A tunable diode laser absorption spectrometer for formaldehyde atmospheric measurements validated by simulation chamber instrumentation, J. Environ. Sci., 24, 22–33, doi:10.1016/S1001-0742(11)60726-2, 2012.

Cazorla, M., Wolfe, G. M., Bailey, S. A., Swanson, A. K., Arkinson, H. L. and Hanisco, T. F.: A new airborne laser-induced fluorescence instrument for in situ detection of formaldehyde throughout the troposphere and lower stratosphere, Atmos. Meas. Tech., 8, 541–552, doi:10.5194/amt-8-541-2015, 2015.

Chance, K., Palmer, P. I., Spurr, R. J. D., Martin, R. V, Kurosu, T. P. and Jacob, D. J.: Satellite observations of formaldehyde over North America from GOME, Geophys. Res. Lett., 27, 3461–3464, doi:10.1029/2000GL011857, 2000.

Co, D. T., Hanisco, T. F., Anderson, J. G. and Keutsch, F. N.: Rotationally resolved absorption cross sections of formaldehyde in the 28100 - 28500 cm^{-1} (351 - 356 nm) spectral region : implications for in situ LIF measurements, J. Phys. Chem. A, 1, 10675–10682, doi: 10.1021/jp053466i, 2005.

Fried, A., Crawford, J., Olson, J., Walega, J., Potter, W., Wert, B., Jordan, C., Anderson, B., Shetter, R., Lefer, B., Blake, D., Blake, N., Meinardi, S., Heikes, B., O'Sullivan, D., Snow, J., Fuelberg, H., Kiley, C. M., Sandholm, S., Tan, D., Sachse, G., Singh, H., Faloona, I., Harward, C. N. and Carmichael, G. R.: Airborne tunable diode laser measurements of formaldehyde during TRACE-P: Distributions and box model comparisons, J. Geophys. Res., 108, 8798, doi:10.1029/2003JD003451, 2003.

Fried, A., Walega, J. G., Olson, J. R., Crawford, J. H., Chen, G., Weibring, P., Richter, D., Roller, C., Tittel, F. K., Heikes, B. G., Snow, J. A., Shen, H., O'Sullivan, D. W., Porter, M., Fuelberg, H., Halland, J. and Millet, D. B.: Formaldehyde over

North America and the North Atlantic during the summer 2004 INTEX campaign: Methods, observed distributions, and measurement-model comparisons, J. Geophys. Res. Atmos., 113, 1–16, doi:10.1029/2007JD009185, 2008a.

Fried, A., Olson, J. R., Walega, J. G., Crawford, J. H., Chen, G., Weibring, P., Richter, D., Roller, C., Tittel, F., Porter, M., Fuelberg, H., Halland, J., Bertram, T. H., Cohen, R. C., Pickering, K., Heikes, B. G., Snow, J. A., Shen, H., O'Sullivan, D. W., Brune, W. H., Ren, X., Blake, D. R., Blake, N., Sachse, G., Diskin, G. S., Podolske, J., Vay, S. A., Shetter, R. E., Hall, S. R., Anderson, B. E., Thornhill, L., Clarke, A. D., McNaughton, C. S., Singh, H. B., Avery, M. A., Huey, G., Kim, S. and Millet, D. B.: Role of convection in redistributing formaldehyde to the upper troposhere over Noth Atlantic during the summer 2004 INTEX campaign, J. Geophys. Res. Atmos., 113, 1–19, doi:10.1029/2007JD009760, 2008b.

Fried, A., Barth, M. C., Bela, M., Weibring, P., Richter, D., Walega, J., Li, Y., Pickering, K., Apel, E., Hornbrook, R., Hills, A., Riemer, D. D., Blake, N., Blake, D. R., Schroeder, J. R., Luo, Z. J., Crawford, J. H., Olson, J., Rutledge, S., Betten, D., Biggerstaff, M. I., Diskin, G. S., Sachse, G., Campos, T., Flocke, F., Weinheimer, A., Cantrell, C., Pollack, I., Peischl, J., Froyd, K., Wisthaler, A., Mikoviny, T. and Woods, S.: Convective transport of formaldehyde to the upper troposphere and lower stratosphere and associated scavenging in thunderstorms over the central United States during the 2012 DC3 study, J. Geophys. Res. Atmos., 121, 7430–7460, doi:10.1002/2015JD024477, 2016.

Hagopian, J.: Carbon nanotubes for stray light suppression, Art. 9417, NASA Tech. Briefs, 2011.

Hak, C., Pundt, I., Kern, C., Platt, U., Dommen, J., Ordóñez, C., Prévôt, a. S. H., Junkermann, W., Astorga-Lloréns, C., Larsen, B. R., Mellqvist, J., Strandberg, A., Yu, Y., Galle, B., Kleffmann, J., Lörzer, J. C., Braathen, G. O. and Volkamer, R.: Intercomparison of four different in-situ techniques for ambient formaldehyde measurements in urban air, Atmos. Chem. Phys., 5, 2897–2945, doi: 10.5194/acp-5-2881-2005, 2005.

Hamill, P., Iraci, L. T., Yates, E. L., Gore, W., Bui, T. P., Tanaka, T. and Loewenstein, M.: A new instrumented airborne platform for atmospheric research, Bull. Am. Meteorogical Soc., 97, 397–404, doi:10.1175/BAMS-D-14-00241.1, 2016.

Hottle, J. R., Huisman, A. J., Digangi, J. P., Kammrath, A., Galloway, M. M., Coens, K. L. and Keutsch, F. N.: Fluorescence-based instrument for in-situ measurements of atmospheric formaldehyde, Environ. Sci. Technol., 43, 790–795, doi: 10.1021/es801621f, 2009.

Jaeglé, L., Jacob, D. J., Brune, W. H. and Wennberg, P. O.: Chemistry of HOx radicals in the upper troposphere, Atmos. Environ., 35, 469–489, doi:10.1016/S1352-2310(00)00376-9, 2001.

Junkermann, W. and Burger, J. M.: A new portable instrument for continuous measurement of formaldehyde in ambient air, J. Atmos. Ocean. Technol., 23, 38–45, doi:10.1175/JTECH1831.1, 2006.

Kaiser, J., Li, X., Tillmann, R., Acir, I., Holland, F., Rohrer, F., Wegener, R. and Keutsch, F. N.: Intercomparison of Hantzsch and fiber-laser-induced-fluorescence formaldehyde measurements, Atmos. Meas. Tech., 7, 1571–1580, doi:10.5194/amt-7-1571-2014, 2014.

Lazrus, A. L., Fong, K. L. and Lind, J. A.: Automated fluorometric determination of formaldehyde in air, Anal. Chem., 60, 1074–1078, doi:10.1021/ac00161a025, 1988.

Luecken, D. J., Hutzell, W. T., Strum, M. L. and Pouliot, G. A.: Regional sources of atmospheric formaldehyde and

acetaldehyde, and implications for atmospheric modeling, Atmos. Environ., 47, 477–490, doi:10.1016/j.atmosenv.2011.10.005, 2012.

Mohlmann, G. R.: Formaldehyde detection in air By laser-induced fluorescence, Appl. Spectrosc., 39, 98–101, doi:10.1366/0003702854249088, 1985.

Olaguer, E. P., Rappenglück, B., Lefer, B., Stutz, J., Dibb, J., Griffin, R., Brune, W. H., Shauck, M., Buhr, M., Jeffries, H., Vizuete, W. and Pinto, J. P.: Deciphering the role of radical precursors during the Second Texas Air Quality Study., J. Air Waste Manag. Assoc., 59, 1258–1277, doi:10.3155/1047-3289.59.11.1258, 2009.

Palmer, P. I., Jacob, D. J., Fiore, A. M., Martin, R. V., Chance, K. and Kurosu, T. P.: Mapping isoprene emissions over North America using formaldehyde column observations from space, J. Geophys. Res., 108, 1984–2012, doi:10.1029/2002JD002153, 2003.

Parrish, D. D., Ryerson, T. B., Mellqvist, J., Johansson, J., Fried, A., Richter, D., Walega, J. G., Washenfelder, R. A., de Gouw, J. A., Peischl, J., Aikin, K. C., McKeen, S. A., Frost, G. J., Fehsenfeld, F. C. and Herndon, S. C.: Primary and secondary sources of formaldehyde in urban atmospheres: Houston Texas region, Atmos. Chem. Phys., 12, 3273–3288, doi:10.5194/acp-12-3273-2012, 2012.

Richter, D., Weibring, P., Walega, J. G., Fried, A., Spuler, S. M. and Taubman, M. S.: Compact highly sensitive multi-species airborne mid-IR spectrometer, Appl. Phys. B Lasers Opt., 119, 119–131, doi:10.1007/s00340-015-6038-8, 2015.

Shim, C., Wang, Y., Choi, Y., Palmer, P. I., Abbot, D. S. and Chance, K.: Constraining global isoprene emissions with Global Ozone Monitoring Experiment (GOME) formaldehyde column measurements, J. Geophys. Res., 110, D24301, doi:10.1029/2004JD005629, 2005.

Steck, T., Glatthor, N., von Clarmann, T., Fischer, H., Flaud, J. M., Funke, B., Grabowski, U., Höpfner, M., Kellmann, S., Linden, A., Perrin, A. and Stiller, G. P.: Retrieval of global upper tropospheric and stratospheric formaldehyde (H_2CO) distributions from high-resolution MIPAS-Envisat spectra, Atmos. Chem. Phys., 8, 463–470, doi:10.5194/acp-8-463-2008, 2008.

Warneke, C., Veres, P., Holloway, J. S., Stutz, J., Tsai, C., Alvarez, S., Rappenglueck, B., Fehsenfeld, F. C., Graus, M., Gilman, J. B. and de Gouw, J. A.: Airborne formaldehyde measurements using PTR-MS: Calibration, humidity dependence, inter-comparison and initial results, Atmos. Meas. Tech., 4, 2345–2358, doi: 10.5194/amt-4-2345-2011, 2011.

Washenfelder, R. A., Attwood, A. R., Flores, J. M., Zarzana, K. J., Rudich, Y. and Brown, S. S.: Broadband cavity-enhanced absorption spectroscopy in the ultraviolet spectral region for measurements of nitrogen dioxide and formaldehyde, Atmos. Meas. Tech., 9, 41–52, doi:10.5194/amt-9-41-2016, 2016.

Weibring, P., Richter, D., Fried, A., Walega, J. G. and Dyroff, C.: Ultra-high-precision mid-IR spectrometer II: system description and spectroscopic performance, Appl. Phys. B Lasers Opt., 85, 207–218, doi:10.1007/s00340-006-2300-4, 2006.

Wert, B. P., Fried, A., Henry, B. and Cartier, S.: Evaluation of inlets used for the airborne measurement of formaldehyde, J. Geophys. Res. Atmos., 107, 4163, doi:10.1029/2001JD001072, 2002.

Yokelson, R. J., Goode, J. G., Ward, D. E., Susott, R. A., Babbitt, R. E., Wade, D. D., Bertschi, I., Griffith, D. W. T. and

Hao, W. M.: Emissions of formaldehyde, acetic acid, methanol, and other trace gases from biomass fires in North Carolina measured by airborne Fourier transform infrared spectroscopy, J. Geophys. Res., 104, 30109–30125, doi:10.1029/1999jd900817, 1999.

Zhu, L., Jacob, D. J., Kim, P. S., Fisher, J. A., Yu, K., Travis, K. R., Mickley, L. J., Yantosca, R. M., Sulprizio, M. P., De Smedt, I., Abad, G. G., Chance, K., Li, C., Ferrare, R., Fried, A., Hair, J. W., Hanisco, T. F., Richter, D., Scarino, A. J., Walega, J., Weibring, P. and Wolfe, G. M.: Observing atmospheric formaldehyde (HCHO) from space: Validation and intercomparison of six retrievals from four satellites (OMI, GOME2A, GOME2B, OMPS) with SEAC4RS aircraft observations over the southeast US, Atmos. Chem. Phys., 16, 13477–13490, doi:10.5194/acp-16-13477-2016, 2016.

St Clair, Jason M. (…, 9/22/2017 2:05 PM
Deleted: Table 1: AJAX flight information with COFFEE in payload, through March 2017.
AJAX flight number ... [2]

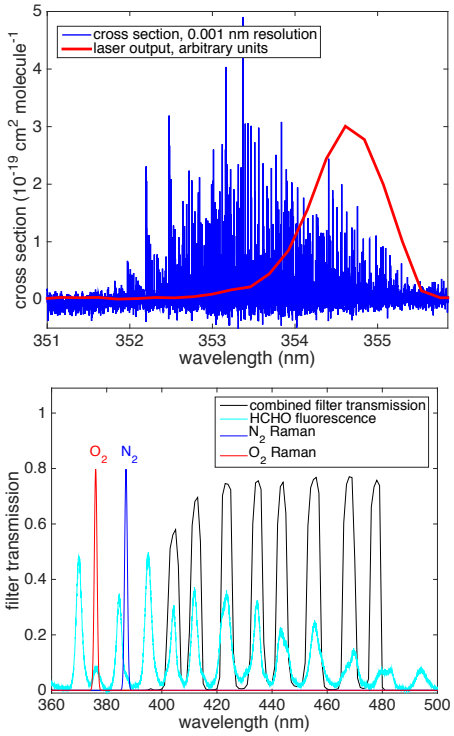

Figure 1: Top Panel: The HCHO absorption spectrum (Co et al., 2005), averaged to 0.001 nm resolution, and the excitation laser spectrum are shown. Bottom Panel: The optical filter transmission spectrum is shown for the detection axis 2 (multi-band pass filter). The HCHO fluorescence and the N_2 and O_2 Raman spectra are included for reference, all with arbitrary units.

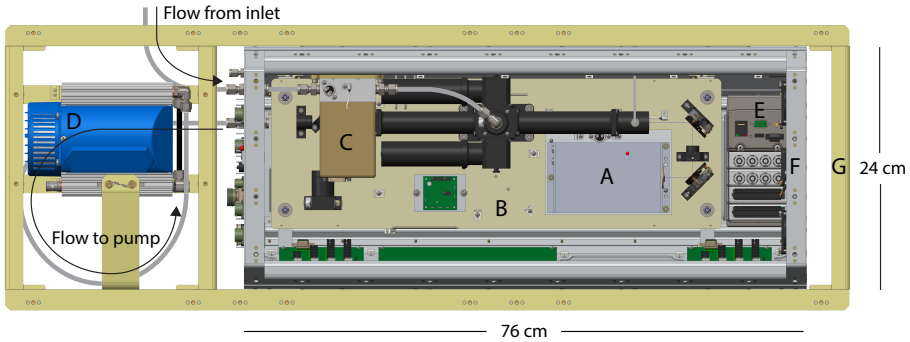

Figure 2: COFFEE instrument layout in the AJAX pod rack, including (A) laser, (B) optical plate, (C) pressure controller, (D) vacuum pump, (E) RIO data acquisition system, (F) instrument chassis, and (G) AJAX pod rack.

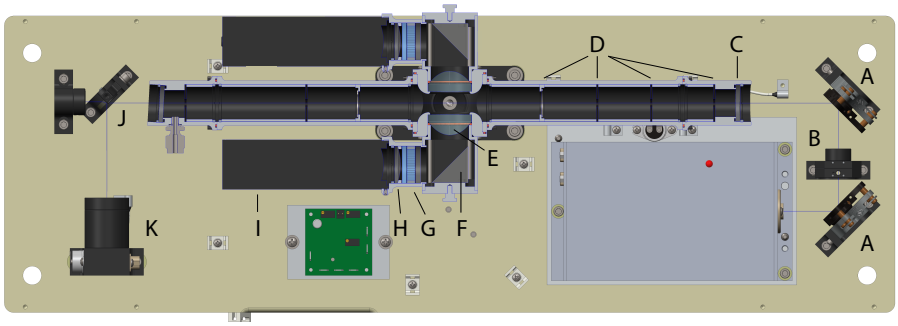

Figure 3: The optical plate layout is shown, with a cut-away of the detection cell. The components include (A) steering mirrors, (B) half-wave plate and collimating lens, (C) cell windows, (D) laser baffles, (E) aspheric lens, (F) prism dielectric mirror, (G) optical filters, (H) lens, (I) photomultiplier tube, (J) beam splitter, and (K) laser power monitor.

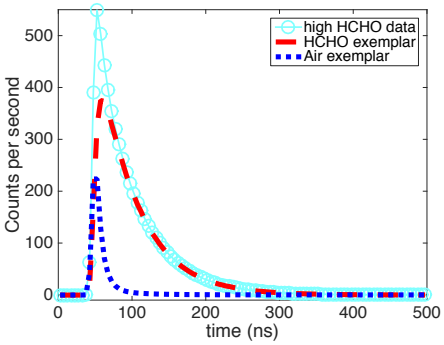

Figure 4: Exemplar time profiles are obtained in the laboratory. The air exemplar is created by averaging the profile with no added HCHO (blue dashed line), and the HCHO exemplar (red dashed line) is obtained by subtracting the air exemplar from data with high (29 ppbv) HCHO (cyan circles).

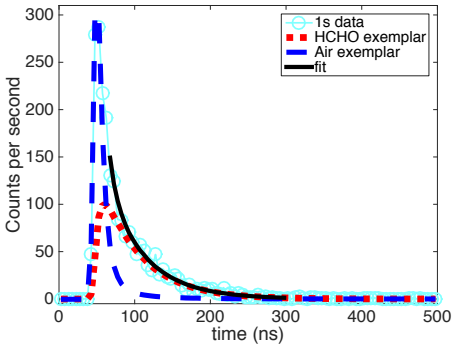

Figure 5: Each 1s data profile (cyan circles) is fit using a linear combination of the air (dashed blue line) and HCHO (dashed red line). The fit profile, over the time window used for the least squares fit, is shown in black. HCHO mixing ratio is 8 ppbv.

St Clair, Jason M. (…, 9/22/2017 2:09 PM
Deleted: . ... [4]

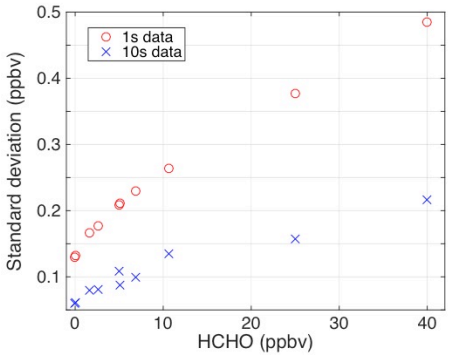

Figure 6: The standard deviation as a function of HCHO is shown to demonstrate the precision of the HCHO measurement for 1 s and 10 s averaging.

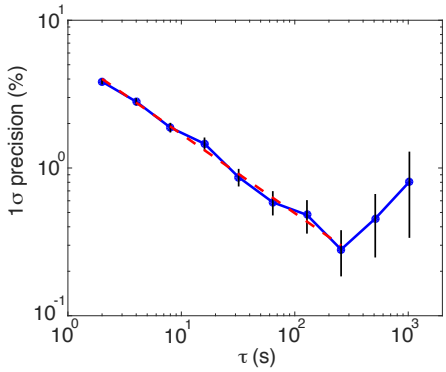

Figure 7: Normalized Allan-Werle deviation as a function of averaging time (τ) demonstrates the precision benefit of time-averaging up to 250 s. Fitting the data with τ < 250 s yields a slope of -0.5 (dashed red line), consistent with white noise dominating the variability at shorter averaging periods. [HCHO] = 5 ppbv.

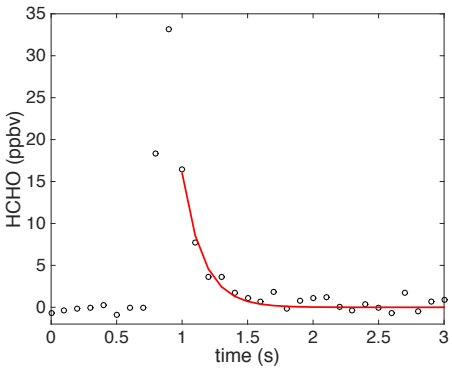

Figure 8: Instrument time response to a pulse of HCHO is fit with an exponential decay, giving an empirical e-fold flush time of 170 ms.

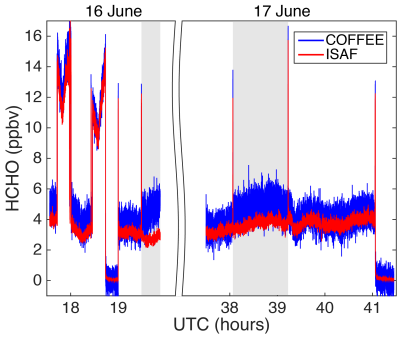

Figure 9: COFFEE (blue) and ISAF (red) data sampling from the roof of Building 33 at GSFC in June 2015. Shaded sections indicate COFFEE sampling without a particle filter. HCHO above 8 ppbv was from sampling indoor air, ~ 4 ppbv was ambient sampling, and ~0 ppbv was through a Drierite/molecular sieve scrubber.

Figure 10: The COFFEE instrument, installed in its AJAX pod rack, is mounted into the mid-body of the inboard left pod.

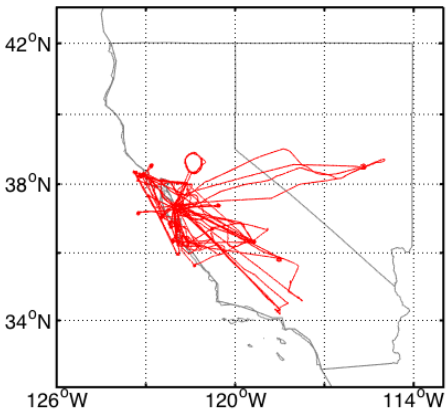

Figure 11: Map of AJAX flight tracks with COFFEE in payload through March 2017.

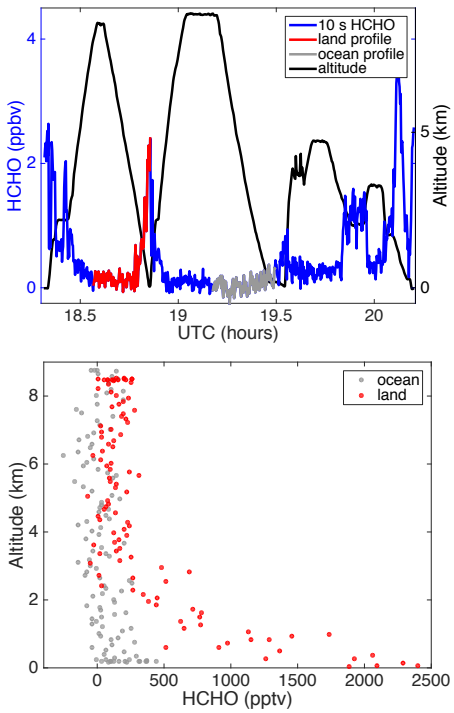

Figure 12: Flight data for AJAX Flight 185 on 2016 April 19. Top Panel: time series of HCHO (10 s data, blue) and the corresponding aircraft altitude (black), with spiral profiles over land (red) and ocean (gray) highlighted. Bottom Panel: altitude profiles of HCHO (10 s data) over land (red) and ocean (gray).